



RESEARCH LETTER

10.1002/2015GL067143

Key Points:

- A study of how the Amundsen Sea Low will change in the future and implications for West Antarctica
- Largest changes in meridional winds found during autumn and winter
- Anthropogenic forcing a key driver of past and future patterns of regional climate change

Supporting Information:

- Supporting Information S1

Correspondence to:

J. S. Hosking,
jask@bas.ac.uk

Citation:

Hosking, J. S., A. Orr, T. J. Bracegirdle, and J. Turner (2016), Future circulation changes off West Antarctica: Sensitivity of the Amundsen Sea Low to projected anthropogenic forcing, *Geophys. Res. Lett.*, *43*, 367–376, doi:10.1002/2015GL067143.

Received 24 NOV 2015

Accepted 10 DEC 2015

Accepted article online 15 DEC 2015

Published online 9 JAN 2016

Future circulation changes off West Antarctica: Sensitivity of the Amundsen Sea Low to projected anthropogenic forcing

J. Scott Hosking¹, Andrew Orr¹, Thomas J. Bracegirdle¹, and John Turner¹

¹British Antarctic Survey, NERC, Cambridge, UK

Abstract The Amundsen Sea Low (ASL) is a major driver of West Antarctic climate variability, with the potential to accelerate the loss of glacial ice. Using the 11 global climate models which most reliably simulate the seasonality in ASL location, we assess the ASL sensitivity to projected future changes using the CMIP5 historical (1951–2000) and representative concentration pathway experiment RCP8.5 (2051–2100). For the first time, we show that the future ASL will likely migrate poleward in summer (December, January, and February) and autumn (March, April, and May), and eastward in autumn and winter (June, July, and August). The autumn–winter changes drive colder southerly winds over the Ross Sea and warmer northerly winds toward the Antarctic Peninsula. This is consistent with recent trends in ERA-Interim reanalysis meridional winds (1979–2014) and reconstructed temperature (1957–2006), suggesting that the impact of anthropogenic forcing on the ASL is likely to play an important role on both past and future patterns of West Antarctic climate variability.

1. Introduction

One of the main factors for West Antarctic surface climate change is the Amundsen Sea Low (ASL), a highly dynamic and mobile climatological low pressure system located in the Pacific sector of the Southern Ocean, between 170–298 E and 80–60 S (Figure 1) [Fogt *et al.*, 2012; Turner *et al.*, 2013; Hosking *et al.*, 2013; Raphael *et al.*, 2015]. In particular, Hosking *et al.* [2013] demonstrated that the longitude of the ASL strongly influences the surface climate by controlling the meridional winds directed toward West Antarctica.

Over recent decades West Antarctica has experienced significant changes in near-surface air temperature [Bromwich *et al.*, 2012], sea ice extent [Turner *et al.*, 2009], snow accumulation [Thomas *et al.*, 2008], and mass balance [McMillan *et al.*, 2014]. These quantities are strongly influenced by changes in the pattern of near-surface winds [Thoma *et al.*, 2008; Turner *et al.*, 2009; Ding *et al.*, 2011; Holland and Kwok, 2012; Dutrioux *et al.*, 2014]. However, due to the large variability in mean sea level pressure (MSLP) in this region [Lachlan-Cope *et al.*, 2001], distinguishing whether such changes are the result of anthropogenic climate change from drivers such as the Antarctic ozone hole or increasing greenhouse gas concentrations (GHGs) or simply within the natural range of the climate system [Polvani and Smith, 2013] is difficult.

Projected future changes of the ASL are therefore a key consideration in determining the response of West Antarctica to changes in stratospheric ozone concentration (which is expected to recover as the Antarctic ozone hole heals) and GHG concentrations (which are expected to increase) [Intergovernmental Panel on Climate Change, 2013]. Previously, Fogt and Zbacnik [2014] concluded that climate models show no clear ozone-related influence on the ASL and surrounding MSLP outside of austral summer. This paper will take a broader perspective by answering the question: How will the mean location of the ASL and associated meridional winds change toward the end of the 21st century (2051–2100) under projected future changes? Such understanding is paramount to improve projections of the mass balance of the West Antarctic ice sheet, which has seen sustained mass losses over recent decades [McMillan *et al.*, 2014] and contains enough ice to raise global sea level by several meters if completely melted [Fretwell *et al.*, 2013].

2. Data and Methods

To assess the sensitivity of the ASL, and the associated wind fields, to projected future changes we analyze seasonal averages of MSLP, 850 hPa geopotential height (Z850) and meridional wind (V850), and zonal winds at

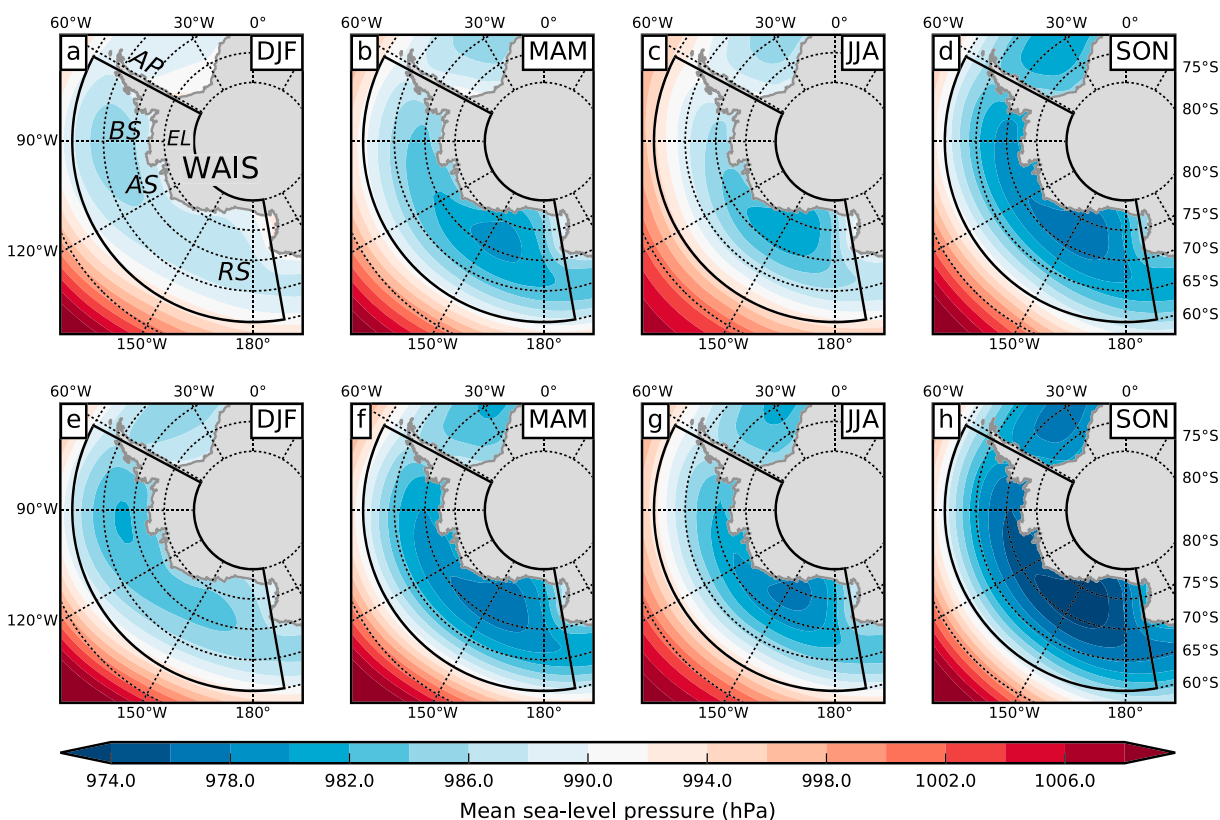


Figure 1. The multimodel seasonal MSLP for the (a–d) CMIP5 historical experiment and (e–h) RCP8.5 averaged over the 50 year periods 1951–2000 and 2051–2100, respectively, based on 11 models with a high skill in simulating the ASL location. The four seasons are shown: (a, e) summer (December–February, DJF), (b, f) autumn (March–May, MAM), (c, g) winter (June–August, JJA), and (d, h) spring (September–November, SON). The domain in which the ASL location is defined is indicated by the drawn box (170–298 E and 80–60 S). Land points are masked out as MSLP is not appropriate over the high orography of West Antarctica. The geographical locations of the regions assessed within this study are highlighted within Figure 1a: West Antarctic Ice Sheet (WAIS), Ellsworth Land (EL), Antarctic Peninsula (AP), Bellingshausen Sea (BS), Amundsen Sea (AS), and Ross Sea (RS).

200 hPa (U200) from the Coupled Model Intercomparison Project Phase 5 (CMIP5) model data set [Taylor *et al.*, 2012] for both the historical period and the RCP8.5 (Representative Concentration Pathway experiment 8.5) future emission scenario. The RCP8.5 experiments correspond to a high-emission scenario of continued GHG increases throughout the 21st century (such that the radiative forcing due to anthropogenic factors reaches 8.5 W m^{-2} by 2100), in combination with stratospheric ozone recovery. The historical experiment includes stratospheric ozone and GHG concentrations representative of the past. Data for the period 1951–2000 in the historical runs and 2051–2100 in the future runs were utilized. The change in the location of the ASL was assessed for each model by analyzing the differences between 50 year climatological seasonal means, i.e., RCP8.5 (2051–2100) minus historical (1951–2000). Models which included more than one ensemble member within an experiment were represented by their ensemble-mean, thereby giving equal weight to each model.

Monthly mean MSLP fields from the European Centre for Medium-Range Weather Forecasts Interim Re-Analysis [ERA-Interim, Dee *et al.*, 2011] are used to validate the representation of the mean annual cycle of ASL longitude and latitude for 49 CMIP5 models over the 27 year overlap period 1979–2005. For each model, we compute the root mean square deviation (RMSD) over all 12 months between the model mean and the reanalysis mean as a single measure of skill (see Figure S1 in the supporting information). A group of models with low RMSD values in both ASL latitude and longitude are selected, namely, CCSM4 [Gent *et al.*, 2011], CESM1-BGC [Hurrell *et al.*, 2013], CESM1-CAM5 [Meehl *et al.*, 2013], CMCC-CM [Scoccimarro *et al.*, 2011], CNRM-CM5 [Volodire *et al.*, 2013], EC-Earth [Hazeleger *et al.*, 2012], GFDL-CM3 [Donner *et al.*, 2011], GFDL-ESM2G [Dunne *et al.*, 2012], HadGEM2-AO [Martin *et al.*, 2011], NorESM1-m, and NorESM1-me [Bentsen *et al.*, 2013]. The MIROC4h [Sakamoto *et al.*, 2012] and MRI-ESM1 [Yukimoto *et al.*, 2012] models were omitted from this selection due to the unavailability of data under the RCP experiment. The MRI-CGCM3 [Yukimoto *et al.*, 2012] model was also omitted due to the large simulated negative bias in regional pressure shown in Hosking *et al.* [2013]. All data

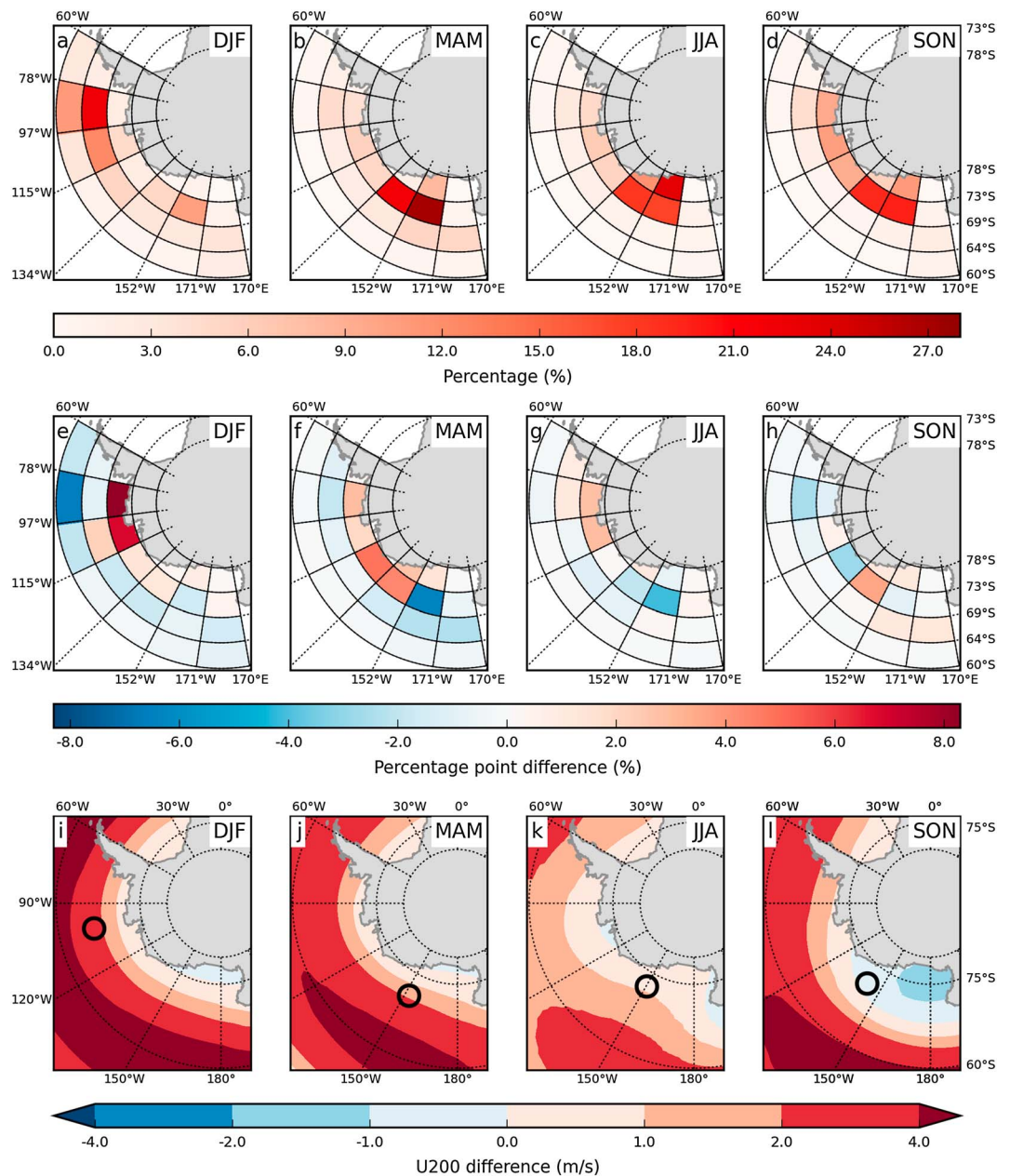


Figure 2. Quantifying simulated ASL location and future shifts for the seasons: (a, e, and i) DJF, (b, f, and j) MAM, (c, g, and k) JJA, and (d, h, and l) SON. The ASL location frequency distribution within the historical experiment (1951–2000) is shown using two-dimensional histograms (Figures 2a–2d). All boxes are of size 18.5° in longitude and 4.5° in latitude. Differences in ASL location between RCP8.5 (2051–2100) and historical experiments are shown in Figures 2e–2h. Blue shading indicates a decrease of the frequency of the ASL being located therein, while red shading indicates an increase. Figures 2i–2l illustrate the differences in U200 where red shading indicates an increase in westerly winds. The median locations of the ASL are highlighted by black unfilled circles.

used to produce multimodel composite maps using the 11 selected models (i.e., Figures 1, 2i–2l, and 3) were spatially regridded to the CMCC-CM model grid (0.75° × 0.75°). The results of this study are largely insensitive to the addition of one or two more models (not shown).

The center position of the ASL was derived by applying a minima finding algorithm (adapted from a peak finding routine developed by SolarSoft [Freeland and Handy, 1998]) to the seasonal MSLP fields over the entire globe. Minima located outside the ASL sector region, defined as 170–298 E, 80–60 S (see Figure 1), were then discarded. The local minimum with the largest amplitude (i.e., the deepest low) was then used to define

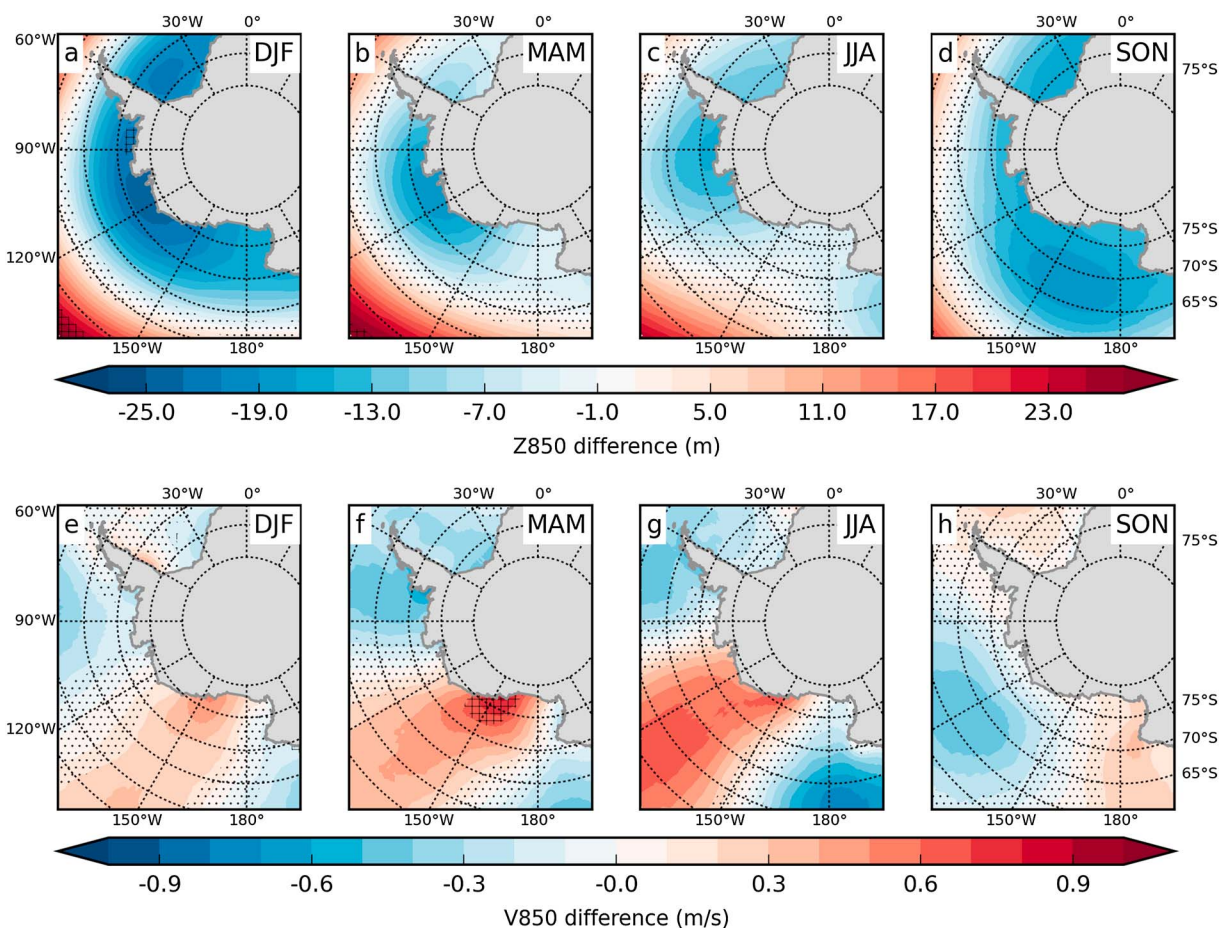


Figure 3. Multimodel mean difference in (a–d) Z850 and (e–h) V850 between the RCP8.5 (2051–2100) and historical (1951–2000) experiments for the four seasons: (a, e) DJF, (b, f) MAM, (c, g) JJA, and (d, h) SON. Blue shading indicates a negative change (decrease in Z850 and southerly shift in V850), while red shading indicates a positive change. Hatching indicates that the change exceeds the level of intermodel spread at the 95% confidence level, while stippling indicates where changes lie below the level of intrinsic variability.

the ASL for that season. Note that as the occurrence of secondary minima within seasonal means was rare, the results were insensitive to whether the primary or (if available) secondary minima were selected as representative of the ASL. This methodology differs from that described in *Hosking et al.* [2013] which defined the location of the ASL as the point of lowest relative central pressure within the ASL sector region, as this occasionally resulted in the center being falsely defined at the boundary edge, even when a well-defined low pressure system was located entirely within the ASL domain. In any case, the results were relatively insensitive to the ASL detection method employed (not shown).

3. Sensitivity of ASL Location to Future Climate Change

Figure 1 shows the climatological seasonal means of the multimodel MSLP for the historical experiment (Figures 1a–1d) and RCP8.5 experiment (Figures 1e–1h). For the historical experiment the mean seasonal cycle is in broad agreement with ERA-Interim climatologies shown by *Turner et al.* [2013] and *Hosking et al.* [2013], showing the ASL located near the Antarctic Peninsula in December–February (DJF), migrating westward in March–May (MAM), and at its deepest in September–November (SON). Comparison with the RCP8.5 results shows that for the period 2051–2100 the MSLP across the Southern Ocean, including the ASL, is reduced by up to ~ 5 hPa (Figures 1e–1h) compared to the historical period, 1951–2000. The reduction in pressure over high latitudes is expected following the projected rise in temperatures in the upper troposphere which will increase faster over the tropics than over the poles. Consequently, the midlatitude circumpolar tropospheric westerly winds are projected to shift poleward and intensify causing the Southern Hemisphere

Annular Mode (SAM) to become more positive [Shindell and Schmidt, 2004]. This is a robust feature across the CMIP5 models [Zheng *et al.*, 2013].

In Figures 2a–2d we show the spatial frequency distribution of the ASL location over the 50 year historical period (1951–2000) using two-dimensional histograms. The locations are *binned* within 28 regional boxes, each spanning an area of 18.5° in longitude and 4.5° in latitude. Although the resulting large-scale spatial patterns are relatively insensitive to the sizes and number of boxes (as highlighted by Figure S2), the histogram grid in Figures 2a–2h was chosen to highlight large-scale patterns across the domain while also capturing changes over the more localized Bellingshausen and Amundsen Sea regions. For each model, these histograms are calculated using all ensemble members individually before converting to percentages. We then average these histograms across the 11 models. As expected, the seasonality of the ASL location frequency within the historical experiment (Figures 2a–2d) is broadly consistent with the area of low pressure in the climatological MSLP fields (Figures 1a–1d). The differences in location frequency between the RCP8.5 experiment and the historical experiment are assessed in panels e–h in Figure 2. Frequency differences of up to eight percentage points are seen around the Antarctic Peninsula in DJF (Figure 2a). In this season, the frequency change is predominately negative over the Southern Ocean and positive nearer the West Antarctic coastline, i.e., consistent with a poleward shift in ASL location. A weaker poleward shift is also evident in MAM (f) and June–August (JJA, g) over the Amundsen–Bellingshausen Sea region. As for ASL longitude, the largest changes are seen during MAM (f), with an eastward shift and differences of up to 5–6 percentage points. By comparison, weaker (3–4 percentage points) shifts are seen in JJA (g) and westward shifts in SON (h).

By assessing the 11 CMIP5 models individually we find that the majority of the models show significant ($p < 0.1$) poleward ASL shifts in DJF and MAM (10 and 8, respectively) with mean values of -1.4 to -0.7° , respectively. Meanwhile the greatest longitudinal shifts are seen in MAM and JJA with around half the models simulating eastward shifts (see Figure S3).

The polar-front jet exit region plays an important role in generating cyclones which in turn underpins the climatological location and depth of the ASL [Fogt *et al.*, 2012]. To determine the underlying driver of future ASL shifts we evaluate U200 differences between RCP8.5 and historical experiments (Figures 2i–2l). The seasons with the largest differences in U200 near the vicinity of the ASL (~ 1 – 4 m s^{-1} , as indicated) are DJF and MAM. These are also the two seasons where we see the strongest poleward ASL shifts. This seasonality is consistent with projected increases in the westerly wind component over the Amundsen Sea shown by Bracegirdle *et al.* [2014], which are largest in DJF and MAM under the RCP8.5 scenarios. The larger zonal wind increases in these seasons are consistent with larger projected increases in the midlatitude to high latitude meridional tropospheric temperature gradient compared to JJA and SON [Bracegirdle *et al.*, 2008]. With regards to longitudinal ASL shifts, the eastward ASL shifts during DJF, MAM, and JJA coincide with westerly U200 changes, while the westward ASL shift during SON coincides with an easterly U200 change (compare Figures 2i–2l with Figure S3). We note however that the strongest U200 changes during DJF do not coincide with the largest longitudinal ASL shift indicating that this is not a linear relationship.

4. Future Change in Near-Surface Circulation

In this section we assess future change in circulation off West Antarctica by assessing climate model output at the 850 hPa level. This enables us to focus on large-scale near-surface changes, while limiting the influence of any model biases linked to sea ice and boundary layer processes.

Future changes in Z850 and V850 in the multimodel mean are shown in Figures 3a–3d and Figures 3e–3h, respectively. These changes are derived by calculating the differences between the RCP8.5 and historical experiments for each model. We then average these fields together to produce the multimodel difference. Regions where the magnitude of the change exceeds 1.96 standard deviations (σ) of the intermodel spread are highlighted by cross hatching. For a two-tailed Student's *t* test, 1.96σ approximates to a significant agreement between model future changes at the 95% confidence level assuming a Gaussian distribution. Similarly, stippling indicates regions where the change is lower than the level of intrinsic variability. Here intrinsic variability is estimated using the multimodel mean standard error calculated from the historical experiment. The standard error statistic is equal to the standard deviation of a sample divided by the square root of the sample size. In the context of this study, for each model the standard deviation of interannual variability over each 50 year time slice is calculated and then divided by the square root of the number of years. This statistic is derived for each model individually before they are averaged together to produce the multimodel mean

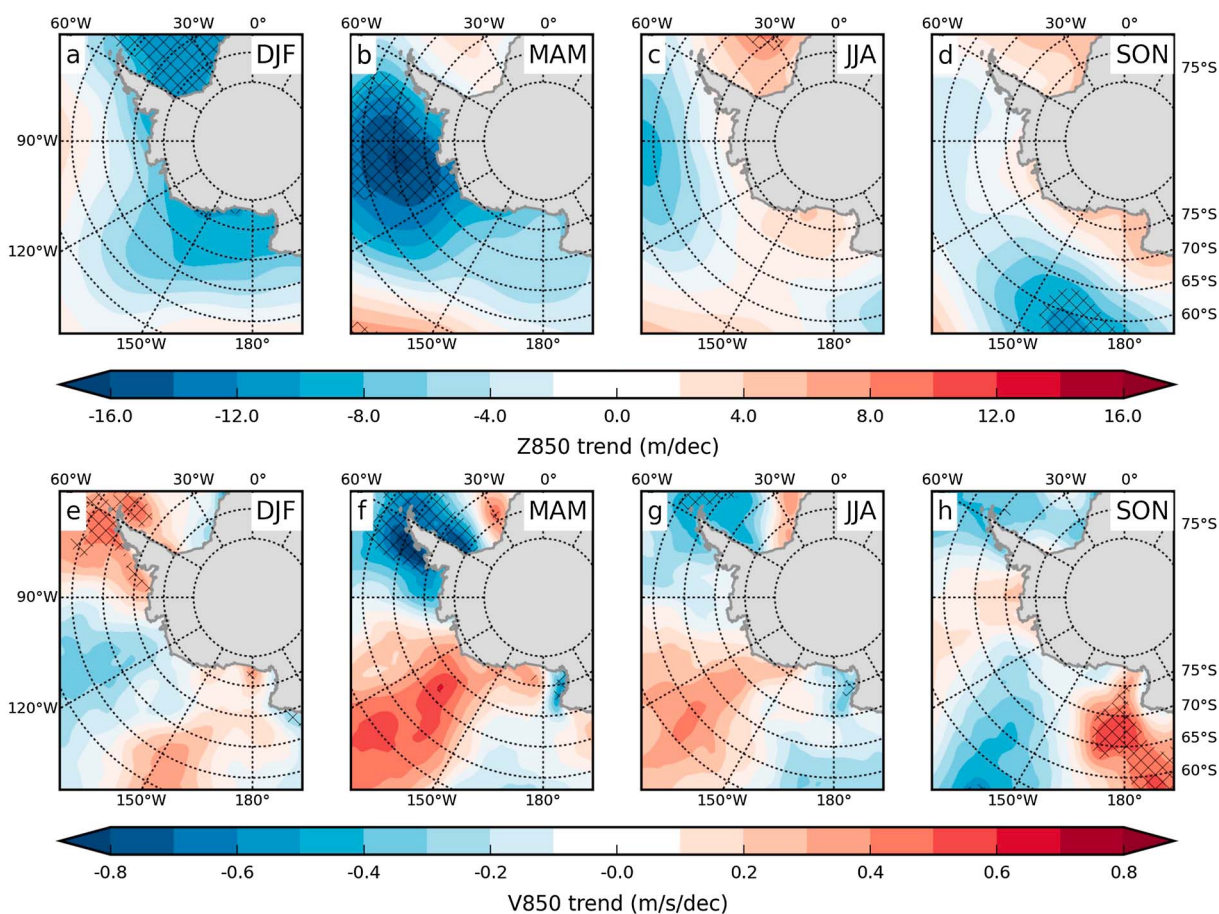


Figure 4. Trends in the ERA-Interim reanalysis fields (a–d) Z850 and (e–h) V850 for the 36 year period 1979–2014 for the four seasons: DJF (a, e), MAM (b, f), JJA (c, g), and SON (d, h). Significant trends ($p < 0.05$) are identified using cross hatching.

standard error. This provides an estimate of the standard deviation of 50 year the means, which is difficult to calculate directly without a large ensemble of runs for each model. Therefore, regions without stippling indicate that the future change (2051–2100) at that location is significantly different to the historical period (1951–2000) and is unlikely to be explained by intrinsic variability.

In Figures 3a–3d, the future Z850 change is broadly negative across the four seasons with the largest reduction in geopotential height found during DJF over the Amundsen Sea (Figure 3a). This is consistent with the strong poleward ASL shift seen in Figure 2a, and the V850 changes (Figure 3e) which have a larger magnitude than the level of intrinsic variability over the eastern Ross Sea and Bellingshausen Sea regions ($\sim 0.4 \text{ m s}^{-1}$).

MAM and JJA (Figures 3b and 3c, respectively) show a decrease in Z850 centered over the Amundsen Sea coast associated with stronger southerly winds over the eastern Ross Sea and northerly winds near the Antarctic Peninsula (Figures 3f and 3g). MAM is the only season with a regional change in which the magnitude is larger than the intermodel spread (eastern Ross Sea), where many of the analyzed models simulate significant ($p < 0.1$) poleward and eastward ASL shifts (respectively, 8 and 5 models. See Figure S3). MAM is therefore the season in which we are most confident of the sign of the meridional wind changes in response to future projected forcing. Unlike the other seasons, future SON V850 changes lie within the bounds of intrinsic variability around the entire West Antarctic coastline. This may be, in part, due to the Z850 change (Figure 3d) being located further north away from the coastline ($\sim 67^\circ\text{S}$ compared to $\sim 73^\circ\text{S}$ in other seasons) preventing the associated increase in meridional winds from reaching West Antarctica. It should be noted that although the reduction in Z850 occurs to the north of the ASL during SON (compare Figure 3d with Figures 1d and 1h), in most models the ASL latitude is insensitive to the projected future forcing in this season (Figure S3).

5. Recent Trends in Near-Surface Circulation

To assess whether the future circulation changes simulated off West Antarctica may have already started we assess ERA-Interim trends in Z850 (Figures 4a–4d) and V850 (Figures 4e–4h) for the period 1979–2014. All comparisons made here between the simulated future changes (i.e., those in Figure 3) and observed past trends are strictly qualitative.

The decreasing trend in Z850 in MAM (Figure 4b) and JJA (Figure 4c) over the Amundsen-Bellingshausen Sea region, along with the associated increase in southerly winds over the eastern Ross Sea and northerly winds over the Peninsula (Figures 4f–4g), are broadly consistent with the spatial patterns of future changes (Figure 3). The observed deepening of Z850 during SON over the north sector of the Ross Sea (Figure 4d) is also consistent. However, there are three significant ($p < 0.05$) V850 features which are less prominent within the future patterns. These are, the southerly winds over the Antarctic Peninsula in DJF (Figure 4e), the northerly winds over the Antarctic Peninsula in MAM (Figure 4f), and the southerly winds over the Ross Sea region in SON (Figure 4h). Previous studies have shown that winds over the Antarctic Peninsula barrier [e.g., *Baines and Fraedrich, 1989; Lefebvre et al., 2004; Orr et al., 2004, 2008; Elvidge et al., 2014*] and the Ross Ice Shelf airstream which forms along the base of the Transantarctic Mountains [e.g., *Parish and Bromwich, 1998; Parish et al., 2006; Steinhoff et al., 2009; Seefeldt and Cassano, 2012; Nigro et al., 2012; Nigro and Cassano, 2014; Coggins et al., 2014*] are modulated by the interaction between large-scale circulation and locally driven orographic processes. The differences between model results and observations over these regions could partly be attributed to the coarse representation of relatively localized orography within global climate models. Therefore, future model projections near the Antarctic Peninsula and Ross Ice Shelf airstream may include a higher degree of uncertainty compared to, e.g., the Amundsen Sea region.

6. Discussion and Conclusions

Rising concentrations in GHG and stratospheric ozone depletion are the main drivers of the observed decreasing pressure around Antarctica which has driven the SAM to become more positive [*Arblaster and Meehl, 2006*]. Previous studies have shown that this trend will continue into the future as GHG concentrations continue to rise, thus further intensifying the westerly winds which flow around Antarctica [*Zheng et al., 2013*]. However, climate variability over West Antarctica is largely driven not by the westerly winds but by the location of the ASL and associated meridional winds [*Hosking et al., 2013; Coggins and McDonald, 2015*]. Therefore, we must turn our attention to the link between these external forcings (GHGs and ozone) and the ASL in order to reduce uncertainties in future projections of West Antarctic climate.

In this study we used 11 CMIP5 coupled atmosphere-ocean models which reliably simulate the ASL location. We compare contrasting 50 year periods from two CMIP5 experiments to assess future ASL change with respect to the present, using the RCP8.5 and historical experiments over the periods 2051–2100 and 1951–2000, respectively. We find that future changes in the strength of the westerly jet (U200) coincide with shifts in the ASL location. The majority of the models simulate significant ($p < 0.1$) poleward ASL shifts in DJF and MAM, while around half of the models simulate significant eastward shifts in MAM and JJA. In these three seasons, future southerly winds are likely to strengthen over the eastern Ross Sea with the change exceeding the level of intrinsic variability. The change in MAM also exceeds the level of intermodel spread (95% confidence). Conversely, changes in meridional winds during SON around the West Antarctic and the peninsula coastline are within the bounds of intrinsic variability (i.e., no robust change).

Surface wind patterns also play an important role in determining Antarctic sea ice concentration and motion [*Stammerjohn et al., 2008; Holland and Kwok, 2012*]. Understanding how the ASL and associated winds have changed over the past three decades may help toward explaining the significant sea ice changes observed off West Antarctica [*Holland, 2014*]. The positive trends in sea ice intensification (the temporal derivative of ice concentration [*Holland, 2014*]) which has occurred during autumn and winter near the ice edge of the eastern Ross Sea region, around 130°W (see Figure 3 in *Holland [2014]*), are thermodynamically and dynamically consistent with the shift to colder southerly winds found in this study.

Until now, the relative contribution of GHGs and stratospheric ozone to such changes in ocean surface winds and sea ice across the West Antarctic sector has been uncertain. Using the UK Met Office Hadley Centre model, *Turner et al. [2009]* found that ozone depletion alone led to a reduction in pressure centered over the Amundsen-Bellingshausen Seas in MAM. A more recent multimodel assessment by *Fogt and Zbacnik [2014]*

concluded that stratospheric ozone depletion had no significant impact on ASL pressure in the lower troposphere outside of austral summer, albeit with a potentially weak response in MAM. However, as other studies have clearly shown that ozone depletion has had no significant impact on the westerly jet beyond the September to January Antarctic ozone hole period [e.g., Orr *et al.*, 2012; Young *et al.*, 2014], it is unlikely that ozone recovery could explain the future ASL shifts during MAM and JJA nor the associated meridional wind changes.

Furthermore, Turner *et al.* [2013] assessed how the ASL location was linked to SAM and El Niño–Southern Oscillation over the reanalysis record. The only significant link was found where SAM in its positive phase was associated with a more poleward ASL. A weak nonsignificant relationship was found where an eastward shift occurs during La Niña events and a westward shift during El Niño events. This is consistent with other studies which found more anomalous low pressure over the Bellingshausen Seas region during La Niña events and high pressure during El Niño events [Karoly, 1989; Lachlan-Cope and Connolley, 2006; Song *et al.*, 2011].

Due to the relatively short satellite observational record, we are not at the stage where we can definitively attribute recent trend patterns to a specific source of large-scale forcing. Nonetheless, the simulated future projections in meridional winds in this study are seasonally and spatially consistent with a previous study of reconstructed surface temperature trend maps for the recent 50 year period 1957–2006 [O'Donnell *et al.*, 2011]—including the warming in MAM and JJA over the Antarctic Peninsula and near Ellsworth land and cooling near the Ross Ice Shelf.

In conclusion, we postulate that the projected changes in meridional winds off the coast of West Antarctica during MAM and JJA are likely to be primarily driven by rising concentrations in GHG, which in turn plays a crucial role in driving regional climate change over the West Antarctic ice sheet. Furthermore, with similar patterns of wind trends also observed over the east Ross Sea region during MAM and JJA over the past 36 years, these changes may have already started.

Acknowledgments

This work was undertaken as part of the Polar Science for Planet Earth Programme of the British Antarctic Survey and funded by the Natural Environment Research Council (NERC) under grant NE/K00445X/1. We acknowledge the World Climate Research Programmes Working Group on Coupled Modelling, which is responsible for CMIP, and we thank the climate modeling groups for producing and making available their model output. For CMIP the U.S. Department of Energy's Program for Climate Model Diagnosis and Intercomparison provides coordinating support and led development of software infrastructure in partnership with the Global Organization for Earth System Science Portals. We acknowledge P. Hick for the development of the peak finding routine which forms part of SolarSoft (<http://www.lmsal.com/solarsoft/>). Many thanks are also given to T. Phillips, G. Marshall, P. Holland, and J. King for valuable discussions on this work.

References

- Arblaster, J. M., and G. A. Meehl (2006), Contributions of external forcings to southern annular mode trends, *J. Clim.*, *19*(12), 2896–2905, doi:10.1175/JCLI3774.1.
- Baines, P. G., and K. Fraedrich (1989), Topographic effects on the mean tropospheric flow patterns around Antarctica, *J. Atmos. Sci.*, *46*(22), 3401–3415.
- Bentsen, M., et al. (2013), The Norwegian Earth system model, NorESM1-M—Part 1: Description and basic evaluation, *Geosci. Model Dev. Discuss.*, *5*(3), 2843–2931, doi:10.5194/gmdd-5-2843-2012.
- Bracegirdle, T. J., W. M. Connolley, and J. Turner (2008), Antarctic climate change over the twenty first century, *J. Geophys. Res.*, *113*, D03103, doi:10.1029/2007JD008933.
- Bracegirdle, T. J., J. Turner, J. S. Hosking, and T. Phillips (2014), Sources of uncertainty in projections of twenty-first century westerly wind changes over the Amundsen Sea, West Antarctica, in CMIP5 climate models, *Clim. Dyn.*, *43*(7), 2093–2104, doi:10.1007/s00382-013-2032-1.
- Bromwich, D. H., J. P. Nicolas, A. J. Monaghan, M. A. Lazzara, L. M. Keller, G. A. Weidner, and A. B. Wilson (2012), Central West Antarctica among the most rapidly warming regions on Earth, *Nat. Geosci.*, *6*(2), 139–145, doi:10.1038/ngeo1671.
- Coggins, J. H. J., and A. J. McDonald (2015), The influence of the Amundsen Sea Low on the winds in the Ross Sea and surroundings: Insights from a synoptic climatology, *J. Geophys. Res. Atmos.*, *120*, 2167–2189, doi:10.1002/2014JD022830.
- Coggins, J. H. J., A. J. McDonald, and B. Jolly (2014), Synoptic climatology of the Ross Ice Shelf and Ross Sea region of Antarctica: K-means clustering and validation, *Int. J. Climatol.*, *34*(7), 2330–2348, doi:10.1002/joc.3842.
- Dee, D. P., et al. (2011), The ERA-Interim reanalysis: Configuration and performance of the data assimilation system, *Q. J. R. Meteorol. Soc.*, *137*(656), 553–597, doi:10.1002/qj.828.
- Ding, Q., E. J. Steig, D. S. Battisti, and M. Küttel (2011), Winter warming in West Antarctica caused by central tropical Pacific warming, *Nat. Geosci.*, *10*(4), 398–403, doi:10.1038/ngeo1129.
- Donner, L. J., et al. (2011), The dynamical core, physical parameterizations, and basic simulation characteristics of the atmospheric component AM3 of the GFDL global coupled model CM3, *J. Clim.*, *24*(13), 3484–3519, doi:10.1175/2011JCLI3955.1.
- Dunne, J. P., et al. (2012), GFDLs ESM2 global coupled climate-carbon Earth System Models. Part I: Physical formulation and baseline simulation characteristics, *J. Clim.*, *25*(19), 6646–6665, doi:10.1175/JCLI-D-11-00560.1.
- Dutrieux, P., J. De Rydt, A. Jenkins, P. R. Holland, H. K. Ha, S. H. Lee, E. J. Steig, Q. Ding, E. P. Abrahamson, and M. Schröder (2014), Strong sensitivity of Pine Island ice-shelf melting to climatic variability, *Science*, *343*(6167), 174–178, doi:10.1126/science.1244341.
- Elvidge, A. D., I. A. Renfrew, J. C. King, A. Orr, and T. A. Lachlan-cope (2014), Foehn warming distributions in nonlinear and linear flow regimes: A focus on the Antarctic Peninsula, *Q. J. R. Meteorol. Soc.*, doi:10.1002/qj.2489.
- Fogt, R. L., and E. A. Zbacnik (2014), Sensitivity of the Amundsen Sea Low to Stratospheric Ozone Depletion, *J. Clim.*, *27*(2012), 9383–9400, doi:10.1175/JCLI-D-13-00657.1.
- Fogt, R. L., A. J. Wovrosh, R. A. Langen, and I. Simmonds (2012), The characteristic variability and connection to the underlying synoptic activity of the Amundsen-Bellingshausen Seas Low, *J. Geophys. Res.*, *117*, D07111, doi:10.1029/2011JD017337.
- Freeland, S. L., and B. N. Handy (1998), Data analysis with the SolarSoft system, *Sol. Phys.*, *182*(2), 497–500, doi:10.1023/A:1005038224881.
- Fretwell, P., et al. (2013), Bedmap2: Improved ice bed, surface and thickness datasets for Antarctica, *Cryosphere*, *7*, 375–393, doi:10.5194/tc-7-375-2013.
- Gent, P. R., et al. (2011), The community climate system model version 4, *J. Clim.*, *24*(19), 4973–4991, doi:10.1175/2011JCLI4083.1.
- Hazeleger, W., et al. (2012), EC-Earth V2.2: Description and validation of a new seamless earth system prediction model, *Clim. Dyn.*, *39*(11), 2611–2629, doi:10.1007/s00382-011-1228-5.

- Holland, P. R. (2014), The seasonality of Antarctic sea ice trends, *Geophys. Res. Lett.*, *41*, 4230–4237, doi:10.1002/2014GL060172.
- Holland, P. R., and R. Kwok (2012), Wind-driven trends in Antarctic sea-ice drift, *Nat. Geosci.*, *5*(12), 872–875, doi:10.1038/ngeo1627.
- Hosking, J. S., A. Orr, G. J. Marshall, J. Turner, and T. Phillips (2013), The influence of the Amundsen-Bellinghousen Seas Low on the climate of West Antarctica and its representation in coupled climate model simulations, *J. Clim.*, *26*, 6633–6648, doi:10.1175/JCLI-D-12-00813.1.
- Hurrell, J. W., et al. (2013), The community earth system model: A framework for collaborative research, *Bull. Am. Meteorol. Soc.*, *94*(9), 1339–1360, doi:10.1175/BAMS-D-12-00121.1.
- Intergovernmental Panel on Climate Change (2013), *Climate change 2013: The Physical Science Basis. Contribution of Working Group I to the Fifth Assessment Report of the Intergovernmental Panel on Climate Change*, 1535 pp., Cambridge Univ. Press, Cambridge, U. K., and New York, doi:10.1017/CBO9781107415324.
- Karoly, D. J. (1989), Southern Hemisphere circulation features associated with El Niño-Southern Oscillation events, *J. Clim.*, *2*, 1239–1252.
- Lachlan-Cope, T. A., and W. M. Connolley (2006), Teleconnections between the tropical Pacific and the Amundsen-Bellinghousen Sea: The role of the El Niño/Southern Oscillation, *J. Geophys. Res.*, *111*, D23101, doi:10.1029/2005JD006386.
- Lachlan-Cope, T. A., W. M. Connolley, and J. Turner (2001), The role of the non-axisymmetric Antarctic orography in forcing the observed pattern of variability of the Antarctic climate, *Geophys. Res. Lett.*, *28*(21), 4111–4114, doi:10.1029/2001GL013465.
- Lefebvre, W., H. Goosse, R. Timmermann, T. Fichefet, H. Goosse, R. Timmermann, T. Fichefet, H. Goosse, R. Timmermann, and T. Fichefet (2004), Influence of the Southern Annular Mode on the sea ice-ocean system, *J. Geophys. Res.*, *109*, C09005, doi:10.1029/2004JC002403.
- Martin, G. M., et al. (2011), The HadGEM2 family of Met Office Unified Model climate configurations, *Geosci. Model Dev.*, *4*(3), 723–757, doi:10.5194/gmd-4-723-2011.
- McMillan, M., A. Shepherd, A. Sundal, K. Briggs, A. Muir, A. Ridout, A. Hogg, and D. Wingham (2014), Increased ice losses from Antarctica detected by CryoSat-2, *Geophys. Res. Lett.*, *41*, 3899–3905, doi:10.1002/2014GL060111.
- Meehl, G. A., W. M. Washington, J. M. Arblaster, A. Hu, H. Teng, J. E. Kay, A. Gettelman, D. M. Lawrence, B. M. Sanderson, and W. G. Strand (2013), Climate change projections in CESM1(CAM5) compared to CCSM4, *J. Clim.*, *26*(17), 6287–6308, doi:10.1175/JCLI-D-12-00572.1.
- Nigro, M. A., and J. J. Cassano (2014), Analysis of the Ross ice shelf airstream forcing mechanisms using self-organizing maps, *Mon. Weather Rev.*, *142*(12), 4719–4734, doi:10.1175/MWR-D-14-00077.1.
- Nigro, M. A., J. J. Cassano, M. A. Lazzara, and L. M. Keller (2012), Case study of a barrier wind corner jet off the coast of the Prince Olav Mountains, Antarctica, *Mon. Weather Rev.*, *140*(7), 2044–2063, doi:10.1175/MWR-D-11-00261.1.
- O'Donnell, R., N. Lewis, S. McIntyre, and J. Condon (2011), Improved methods for PCA-based reconstructions: Case study using the Steig et al. (2009) Antarctic temperature reconstruction, *J. Clim.*, *24*(8), 2099–2115, doi:10.1175/2010JCLI3656.1.
- Orr, A., D. Cresswell, G. J. Marshall, J. C. R. Hunt, J. Sommeria, C. Wang, and M. Light (2004), A 'low-level' explanation for the recent large warming trend over the western Antarctic Peninsula involving blocked winds and changes in zonal circulation, *Geophys. Res. Lett.*, *31*, L06204, doi:10.1029/2003GL019160.
- Orr, A., G. J. Marshall, J. C. R. Hunt, J. Sommeria, C.-G. Wang, N. P. M. van Lipzig, D. Cresswell, and J. C. King (2008), Characteristics of summer airflow over the Antarctic Peninsula in response to recent strengthening of westerly circumpolar winds, *J. Atmos. Sci.*, *65*, 1396–1413.
- Orr, A., T. J. Bracegirdle, J. S. Hosking, T. Jung, J. D. Haigh, T. Phillips, and W. Feng (2012), Possible dynamical mechanisms for Southern Hemisphere climate change due to the ozone hole, *J. Atmos. Sci.*, *69*(10), 2917–2932, doi:10.1175/JAS-D-11-0210.1.
- Parish, T. R., and D. H. Bromwich (1998), A case study of Antarctic Katabatic Wind interaction with large-scale forcing, *Mon. Weather Rev.*, *126*(1), 199–209, doi:10.1175/1520-0493(1998)126<0199:ACSOAK>2.0.CO;2.
- Parish, T. R., J. J. Cassano, and M. W. Seefeldt (2006), Characteristics of the Ross Ice Shelf air stream as depicted in Antarctic Mesoscale Prediction System simulations, *J. Geophys. Res.*, *111*, D12109, doi:10.1029/2005JD006185.
- Polvani, L. M., and K. L. Smith (2013), Can natural variability explain observed Antarctic sea ice trends? New modeling evidence from CMIP5, *Geophys. Res. Lett.*, *40*, 3195–3199, doi:10.1002/grl.50578.
- Raphael, M. N., G. J. Marshall, J. Turner, R. Fogt, D. Schneider, D. A. Dixon, J. S. Hosking, J. M. Jones, and W. R. Hobbs (2015), The Amundsen Sea Low: Variability, change and impact on Antarctic Climate, *Bull. Am. Meteorol. Soc.*, doi:10.1175/BAMS-D-14-00018.1.
- Sakamoto, T. T., et al. (2012), MIROC4h—A new high-resolution atmosphere-ocean coupled general circulation model, *J. Meteorol. Soc. Jpn.*, *90*(3), 325–359, doi:10.2151/jmsj.2012-301.
- Scoccimarro, E., S. Gualdi, A. Bellucci, A. Sanna, P. G. Fogli, E. Manzini, M. Vichi, P. Oddo, and A. Navarra (2011), Effects of tropical cyclones on ocean heat transport in a high-resolution coupled general circulation model, *J. Clim.*, *24*(16), 4368–4384, doi:10.1175/2011JCLI4104.1.
- Seefeldt, M. W., and J. J. Cassano (2012), A description of the Ross Ice Shelf air stream (RAS) through the use of self-organizing maps (SOMs), *J. Geophys. Res.*, *117*, D09112, doi:10.1029/2011JD016857.
- Shindell, D. T., and G. A. Schmidt (2004), Southern Hemisphere climate response to ozone changes and greenhouse gas increases, *Geophys. Res. Lett.*, *31*, L18209, doi:10.1029/2004GL020724.
- Song, H.-J., E. Choi, G.-H. Lim, Y. H. Kim, J.-S. Kug, and S.-W. Yeh (2011), The central Pacific as the export region of the El Niño-Southern Oscillation sea surface temperature anomaly to Antarctic sea ice, *J. Geophys. Res.*, *116*, D21113, doi:10.1029/2011JD015645.
- Stammerjohn, S., D. G. Martinson, R. C. Smith, X. Yuan, and D. Rind (2008), Trends in Antarctic annual sea ice retreat and advance and their relation to El Niño-Southern Oscillation and Southern Annular Mode variability, *J. Geophys. Res.*, *113*, C03S90, doi:10.1029/2007JC004269.
- Steinhoff, D. F., S. Chaudhuri, and D. H. Bromwich (2009), A case study of a Ross ice shelf airstream event: A new perspective, *Mon. Weather Rev.*, *137*, 4030–4046, doi:10.1175/2009MWR2880.1.
- Taylor, K. E., R. J. Stouffer, and G. A. Meehl (2012), An overview of CMIP5 and the experiment design, *Bull. Am. Meteorol. Soc.*, *93*(4), 485–498, doi:10.1175/BAMS-D-11-00094.1.
- Thoma, M., A. Jenkins, D. Holland, and S. Jacobs (2008), Modelling circumpolar deep water intrusions on the Amundsen Sea continental shelf, Antarctica, *Geophys. Res. Lett.*, *35*, L18602, doi:10.1029/2008GL034939.
- Thomas, E. R., G. J. Marshall, and J. R. McConnell (2008), A doubling in snow accumulation in the western Antarctic Peninsula since 1850, *Geophys. Res. Lett.*, *35*, L01706, doi:10.1029/2007GL032529.
- Turner, J., J. C. Comiso, G. J. Marshall, T. A. Lachlan-Cope, T. Bracegirdle, T. Maksym, M. P. Meredith, Z. Wang, and A. Orr (2009), Non-annular atmospheric circulation change induced by stratospheric ozone depletion and its role in the recent increase of Antarctic sea ice extent, *Geophys. Res. Lett.*, *36*, L08502, doi:10.1029/2009GL037524.
- Turner, J., T. Phillips, J. S. Hosking, G. J. Marshall, and A. Orr (2013), The Amundsen Sea low, *Int. J. Climatol.*, *33*(7), 1818–1829, doi:10.1002/joc.3558.
- Voldoire, A., et al. (2013), The CNRM-CM5.1 global climate model: Description and basic evaluation, *Clim. Dyn.*, *40*(9–10), 2091–2121, doi:10.1007/s00382-011-1259-y.
- Young, P. J., S. M. Davis, B. Hassler, S. Solomon, and K. H. Rosenlof (2014), Modeling the climate impact of Southern Hemisphere ozone depletion: The importance of the ozone data set, *Geophys. Res. Lett.*, *41*, 9033–9039, doi:10.1002/2014GL061738.

- Yukimoto, S., et al. (2012), A new global climate model of the meteorological research institute: MRI-CGCM3 -Model description and basic performance-, *J. Meteorol. Soc. Jpn.*, 90A, 23–64, doi:10.2151/jmsj.2012-A02.
- Zheng, F., J. Li, R. T. Clark, and H. C. Nnamchi (2013), Simulation and projection of the Southern Hemisphere annular mode in CMIP5 models, *J. Clim.*, 26(24), 9860–9879, doi:10.1175/JCLI-D-13-00204.1.